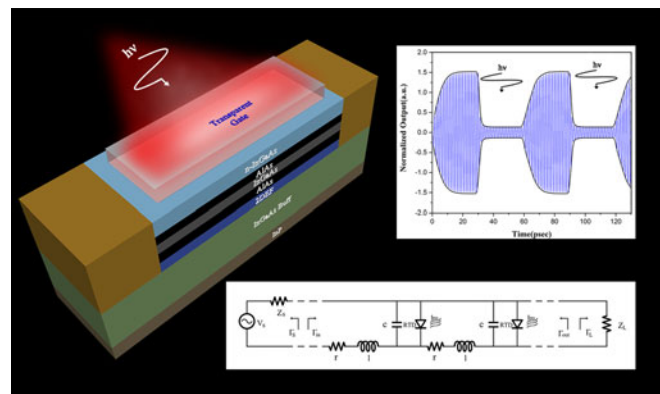


Photocontrolled Terahertz Amplified Modulator via Plasma Wave Excitation in ORTD-Gated HEMTs

Volume 9, Number 5, October 2017

Changju Zhu
Luhong Mao
Fan Zhao
Xurui Mao
Weilian Guo



DOI: 10.1109/JPHOT.2017.2752841
1943-0655 © 2017 IEEE

Photocontrolled Terahertz Amplified Modulator via Plasma Wave Excitation in ORTD-Gated HEMTs

Changju Zhu,¹ Luhong Mao,¹ Fan Zhao,¹ Xurui Mao,²
and Weilian Guo¹

¹School of Electrical and Information Engineering, Tianjin University, Tianjin 300072, China

²State Key Laboratory on Integrated Optoelectronics, Institute of Semiconductors, Chinese Academy of Sciences, Beijing 100083, China

DOI:10.1109/JPHOT.2017.2752841

1943-0655 © 2017 IEEE. Translations and content mining are permitted for academic research only.
Personal use is also permitted, but republication/redistribution requires IEEE permission.
See http://www.ieee.org/publications_standards/publications/rights/index.html for more information.

Manuscript received September 5, 2017; accepted September 11, 2017. Date of publication September 15, 2017; date of current version October 9, 2017. This work was supported by the National Key Research and Development Program of China under Grant 2016YFA0202201. Corresponding authors: Luhong Mao; Xurui Mao (e-mail: lhmao@tju.edu.cn; maoxurui@semi.ac.cn).

Abstract: This paper theoretically explores photocontrolled terahertz amplified modulator in electron plasma wave optically switched resonant tunneling diode (ORTD) gate high-electron mobility transistor. We present a developed distributed circuit model based on the Khmyrova model. Photoexcitation causes ORTD operating state between negative differential conductivity and positive differential conductivity, which power gain of the device can be controlled by photoexcitation. Numerical and analytical results show that photoexcitation enabling amplified modulator can realize much larger modulation depth (>95%) than what has been reported in photocontrolled modulator. Our results show the potential of this device in several fields of terahertz technology, such as photocontrolled modulator, mixer, and other two port networks.

Index Terms: Optically switched resonant tunneling diode (ORTD), high-electron mobility transistor (HEMT), photo-controlled, amplified modulator

1. Introduction

Terahertz electromagnetic waves, lying at the boundary between microwave and infrared wave, has many excellent features, such as better penetrability, its ability to observe inter-molecular vibrations [1]. Due to its inherent unique properties, terahertz technology attracts much of attention in astronomy, spectroscopy, wireless communication, imaging, etc [2]–[4]. Two-dimensional electron gas materials, including heterostructure [5]–[7] and graphene [8]–[10] with remarkable optoelectronic properties in terahertz band, become very promising materials to develop terahertz devices, such as modulators, amplifier, and so on. Generally speaking, electrical-controlled modulators have only approximately 10 MHz modulation bandwidth [11]–[13]. Photo-controlled terahertz modulators combined with ultrafast laser can achieve over 1 GHz modulation bandwidth [14]–[16]. Photo-controlled modulators, using two-dimensional electron gas materials, are very promising device in terahertz communication.

In this paper, we study the possibility of a plasmonic terahertz amplified modulator basing on photo-controlled functions. In architecture of the device, amplified modulation originates from the different operating state of the optically switched resonant tunneling diode (ORTD) between the

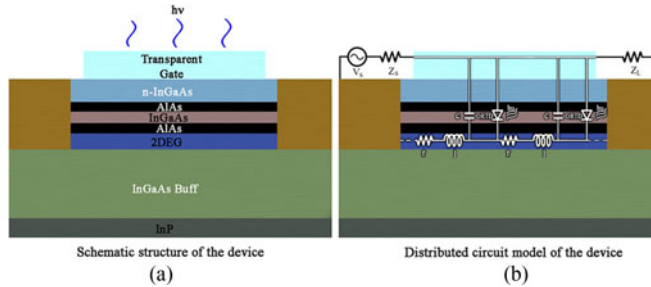


Fig. 1. (a) Schematic structure of the device, n-InGaAs layer is the light absorption layer; (b) distributed circuit model of the device, V_S represents the input sign, Z_S and Z_L represents the impedance of source and load.

negative differential conductivity (NDC) and positive differential conductivity (PDC) by photo excitation. As discussed by Sensale-Rodriguez in their works [6], [7], [18], the NDC can compensate for the loss of the electron-plasma-waves in high-electron mobility transistor (HEMT) channel, which forms a gain medium at terahertz frequencies. ORTD combination with ultrafast lasers, which can deliver optical pulses of <1 ps pulse width, is suitable to develop a ultrafast THz modulator [19]. By means of numerical simulation for ORTD-gated HEMTs, we show that (I) the mechanism of the photo-controlled amplified modulator, (II) the difference of power gain between photo-excitation and non-photo-excitation, (III) the power density of the photo-excitation is an important parameter to the modulator depth level, signal bandwidth as well as high level voltage.

2. Modeling

Structure of the device is shown in Fig. 1. The material system of HEMT is InGaAs. A double barrier structure (DBS) consists of a thick InGaAs quantum well and two thick AlAs barriers. The plasma wave in the channel of the HEMT is under the DBS. The n-InGaAs layer is light absorption layer on the DBS. A polymer electrolyte poly (ethylene oxide) and LiClO₄) layer, as light window, was spin-coated on the entire chip [20]. The light absorption layer generates electron-hole parts by Photo-excitation. Photo-excited electron-hole parts subjected by an electric field in biased ORTD become locally separated [21], [22], which cause a shift on the I-V curves of ORTD. We bias ORTD-gate HEMT at the maximum NDC point to realize maximum power gain. The optical modulation mechanism is based on the scenario that photo-excitation causes a shift of ORTD operating state from NDC to PDC. The power gain of the device decreases under this condition, which causes intensity modulation.

According to Beown *et al.* [23] theory, the effects of photo-excitation on ORTD I-V curve can be described by:

$$J = A \ln \left(\frac{1 + e^{B-C+n_1(V+V_{ph})q/kT}}{1 + e^{B-C-n_1(V+V_{ph})q/kT}} \right) \left(\frac{\pi}{2} + \arctan \left(\frac{C - n_1(V + V_{ph})}{D} \right) \right) + He^{\frac{n_2 q(V+V_{ph})}{kT} - 1} \quad (1)$$

where J is the current intensity, V_{ph} is a photoinduced voltage due to the charge accumulation effect, q is the electron charge, k is Boltzmann's constant, T is thermodynamic temperature, A is the peak current density, $B = \frac{E_F}{q}$ (where E_F is the Fermi level in the emitter), $C = \frac{E_r}{q}$ (where E_r is the ground state level in the quantum well), $D = \frac{\Gamma}{2}$ (where Γ is the resonance width), H is reverse saturation current density, and n_1 , n_2 is fitting coefficients to $I - V$ curve under dark condition. The fitting coefficients are: $A = 1.2067e + 10A/m^2$, $B = 0.085$ V, $C = 0.1334$ V, $D = 0.1$ V, $H = 7.7600e + 10A/m^2$, $n_1 = 0.1502$, $n_2 = 0.0041$. Under photo-excitation, V_{ph} is given by [24] :

$$V_{ph} = \frac{\Delta n}{c_0} = \frac{\alpha \tau l d}{c_0 h v} (1 - e^{-\frac{1}{\tau}}) \quad (2)$$

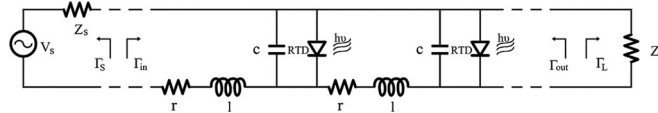


Fig. 2. Equivalent circuit for analysis for an ORTD-gated plasma wave HEMT.

where Δn is the rate of the photon-generated carrier, d is the thickness of the gate, h is Planck's constant, α is the absorption coefficient of n-GaAlAs, τ is lifetime of photon-generated carrier, v , I is frequency and power density of the photo-excitation, c_0 is the capacitance per unit area of gate.

According to Dyakonov and Shur theory [25], [26], plasma wave in the channel of the HEMT behaves like two-dimensional electron fluid (2DEF). The 2DEF can be described by a hydrodynamic model. Providing appropriate electrical boundary conditions, the plasma wave can be continuously increased until it's limited by the mechanism of energy loss. For a typical submicron GaAlAs HEMT, the group velocity of plasma waves is larger than the electron drift velocity, whose characteristic frequency is in the Terahertz band [27]. Fundamental characteristic frequency f is given by:

$$f = \frac{\Omega}{2\pi} = \frac{1}{2L} \sqrt{\frac{\pi e^2}{\epsilon_r m^*}} \quad (3)$$

where Ω is the characteristic angular frequency of plasma wave, e and m^* is the electron charge and effective mass, ϵ_r is the dielectric constant of gate, L is the gate length. The width of the device is $20 \mu\text{m}$ in the simulation. Here we considered $L = 300 \text{ nm}$ as the gate length in the design, which characteristic frequency is 718 GHz.

Due to similarity of electromagnetic wave propagation in the channel of 2DEG-gate HEMT structure, a transmission line model explicitly employed to model of high-frequency effects in such a 2DEG system by Burke *et al.* [28]. In this paper, to facilitate the amplified modulator design, a distributed circuit model has been developed based on Khmyrova model [27], as shown in Fig. 2. V_s with the impedance Z_s represents the input terahertz signal source, and Z_L represents the load between drain and gate. In small-signal approximation, ORTD can be regarded as a differential conductance g . The distributed circuit model has similarity with a transmission line, which contain distributed resistance r , kinetic inductance l , gate capacitance c and differential conductance of ORTD g [27]:

$$r = \frac{1}{e\mu n_s W} \quad (4)$$

$$l = \frac{m^*}{e^2 \mu n_s W} \quad (5)$$

$$c = c_0 W \quad (6)$$

$$g = g_0 W = W \frac{\partial J}{\partial V} \quad (7)$$

where μ is electron mobility of GaAlAs, V is the bias voltage of the gate, W is the gate width. A transmission line propagation constant and characteristic impedance can define as [29]:

$$\gamma = \sqrt{(r + j\omega l)(g + j\omega c)} \quad (8)$$

$$Z = \sqrt{\frac{r + j\omega l}{g + j\omega c}} \quad (9)$$

where ω is the angular frequency. To a two-port network, the transducer power gain G_T is given by:

$$G_T = \frac{|S_{21}|^2 (1 - |\Gamma_S|^2)(1 - |\Gamma_L|^2)}{|1 - \Gamma_S \Gamma_L|^2 |1 - S_{22} \Gamma_L|^2} \quad (10)$$

where

$$S_{11} = S_{22} = \frac{\xi \sinh(\gamma L) - \xi^{-1} \sinh(\gamma L)}{2 \cosh(\gamma L) + \sinh(\gamma L)(\xi + \xi^{-1})} \quad (11)$$

$$S_{12} = S_{21} = \frac{2}{2 \cosh(\gamma L) + \sinh(\gamma L)(\xi + \xi^{-1})} \quad (12)$$

$$\Gamma_{in} = S_{11} + \frac{S_{21} S_{21} \Gamma_L}{1 - S_{22} \Gamma_L} \quad (13)$$

$$\xi = \frac{Z}{Z_0} \quad (14)$$

where Γ_S and Γ_L is the source and load reflection coefficients with respect to $Z_0 = 50 \Omega$, Γ_{in} is reflection coefficient of the input, S_{11} is return loss and S_{21} is transmission gain. The maximum transducer power gain occurs in a specific case where the input and output matched. In this condition, $\Gamma_S = \Gamma_L = 0$, transducer power gain can be simplified as

$$G_T = |S_{21}|^2 \quad (15)$$

In amplitude modulation, the terahertz signal $m(t)$ is impressed on the amplitude of the carrier signal $c(t) = S_{21}(t)$ [30]. The amplitude modulated $u(t)$ signal is obtained by multiplying by $m(t)$ and $c(t)$

$$u(t) = m(t) \times S_{21}(t) \quad (16)$$

The $S_{21}(t)$ changes by photo-excitation and is facilitated by two state, non-photo-excitation state S_{21}^1 and photo-excitation S_{21}^2 . The $u(t)$ can be simplified as

$$u(t) = \begin{cases} m(t) S_{21}^1, & \text{non - photo - excitation} \\ m(t) S_{21}^2, & \text{photo - excitation} \end{cases} \quad (17)$$

The modulation depth M_T of the modulator can be defined by [31]:

$$M_T = \frac{T_{max} - T_{min}}{T_{max}} \times 100\% \quad (18)$$

where T_{max} and T_{min} is the maximum and minimum of the intensity. In this paper, the modulation depth is

$$M_T = \frac{|S_{21}^1| - |S_{21}^2|}{|S_{21}^1|} = \frac{\sqrt{G_T^1} - \sqrt{G_T^2}}{\sqrt{G_T^1}} \quad (19)$$

where $\sqrt{G_T^1}$ is the transducer power gain in non-photo-excitation, $\sqrt{G_T^2}$ is the transducer power gain in photo-excitation. As can be seen, by in (19), that decreasing $\sqrt{G_T^2}$ is a necessary condition to achieve large modulation depth.

3. Simulation and Discussion

In our simulation, device physical parameters are listed in Table I. Fig. 3(a) shows the $I - V$ curve of ORTD at non-photo-excitation and different photo-excitation. Firstly, supposed that the device is set at the maximum NDC point when no photo-excitation, the return loss S_{11} being very small, the S_{21} parameter realize maximum gain 4.28 dB which the transducer power gain is 8.56 dB. When the device is photo-excited, the photo-excitation causes a shift on the $I - V$ curve of ORTD. This causes the ORTD operating-state swinging from NDC region to PDC region, as shown in Fig. 3(b). Under the influence of the photo-excitation, absolute value of NDC decreasing, the ability of NDC in the gate to counteract the friction (distributed resistance r) of the plasma wave in the channel is

TABLE I
Device Parameter [27], [32]–[34]

Parameters	Value
Electron Mobility μ	$27000 \text{ cm}^2 \text{V}^{-1} \text{s}^{-1}$
2DEG Sheet Electron Density n_s	10^{12} cm^{-2}
Average Lifetime of Optically Excited Carriers τ	2.58 ps
Electron Effective Mass m^*	$0.036 m_0$
Dielectric Constant of Gate ϵ_r	12
Photo-excitation frequency ν	474 THz
Absorption Coefficient α	5.52×10^6

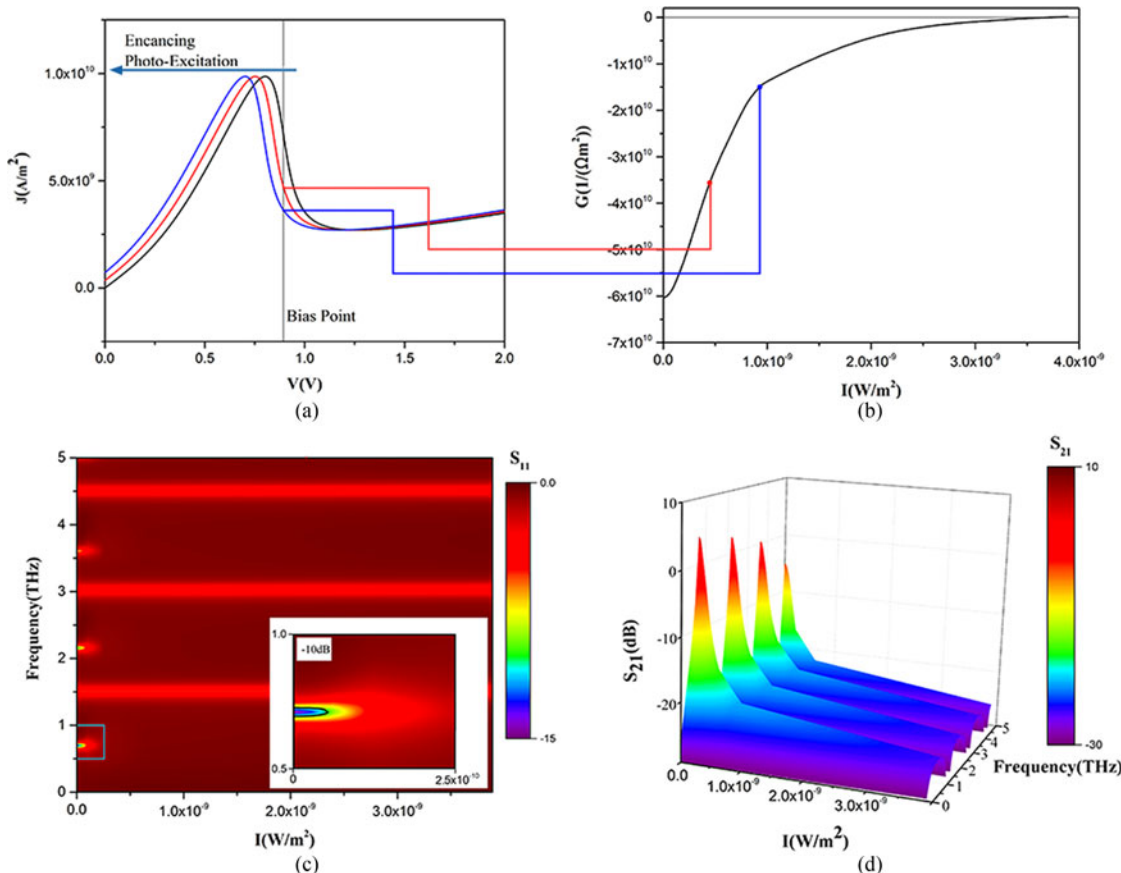


Fig. 3. (a) ORTD current as a function of gate voltage without photo-excitation. Black line is non-photo-excitation condition; color lines are photo-excitation condition. (b) Differential conductance as a function of the photo-excitation; (c) S_{11} parameter as a function of the photo-excitation and frequency. The $S_{11} < -10 \text{ dB}$ is in black district of the partial magnification between 0.5–1 THz and 0 – $2.5 \times 10^{-10} \text{ W/m}^2$; (d) S_{21} parameter as a function of the photo-excitation and frequency.

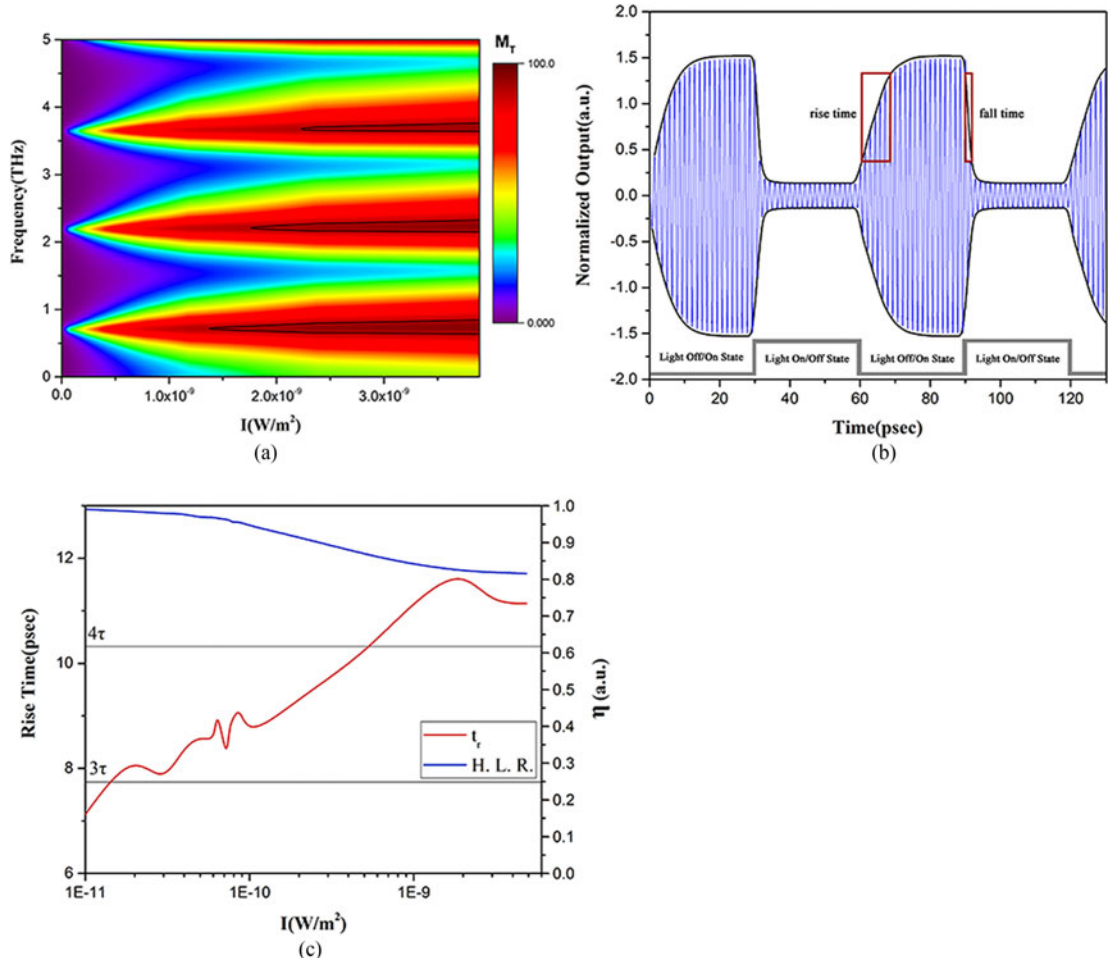


Fig. 4. (a) The effect of photo-excitation on modulation depth. The areas inside the black lines are $M_T > 90\%$; (b) the Signals envelope as a function of time. The period of photo-excitation is 60 ps; the rise time is about 8.4 ps and the fall time is about 2 ps. (c) The effects of photo-excitation on t_r and high-level voltage receding.

decreasing. The energy loss of plasma wave is increasing, return loss increasing, which cause S_{21} as well as power gain deteriorating, as shown in Fig. 3(c) and (d).

As analyzed above, the power gain of the device decreases under photo-excitation since the operating condition is moved from NDC to PDC. This causes intensity modulation. The effect of photo-excitation on modulation depth is shown in Fig. 4(a). The modulation depth increases effectively with the increasing of photo-excitation. However, enhancing the power density of the light, the power gain of the device deteriorates, as shown in Fig. 3(d). This causes T_{\min} becoming smaller and T_{\max} alter little. Numerical simulation may help to make the tradeoff and it shows that under proper photo-excitation density, the modulation depth can realize $>95\%$. The modulation rate is limited by the lifetime life of photogenerated carrier τ . As shown in Fig. 4(b), rise time of the device is much large than fall time. During photo-excitation, the photoinduced voltage V_{ph} (see (2)) need very little time to rise large enough. However, V_{ph} needs $>3\tau$ to drop to a negligible size in decay process after photo-excitation, in which the signal bandwidth $W_B = 0.35/t_r$ is above 40 GHz. V_{ph} in decay process still have a tiny one after long time, which may cause magnitude of high level voltage decreasing after large photo-excitation. To describe magnitude of high level voltage decreasing after photo-excitation, we use the voltage-decay rate η by:

$$\eta = \frac{V_1}{V_0} \quad (20)$$

where V_0 is the voltage without photo-excitation, V_1 is the high level voltage induced by photo-excitation. A tiny photoinduced voltage causes magnitude of high level voltage decreasing without photo-excitation, and causes rise time increased, as shown in Fig. 4(c). These results show that modulation depth of device is much larger than optical modulator [14]–[16] and operating frequency as well as bandwidth is much larger than electrical modulator [11]–[13].

4. Conclusions

To conclude, this paper demonstrates the possibility of photo-controlled terahertz amplified modulator based on plasma wave ORTD-gate HEMT. Photo-excitation causes a shift on I-V curve of the ORTD, absolute value of NDC decreasing. This leads to a deteriorating in the power gain, which cause amplitude modulation. With appropriate photo-excitation, the modulator can realize an extremely high modulation depth (>95%) with the power gain >8 dB and a broad bandwidth (>40 GHz). On account of its outstanding performances, the photo-controlled plasmonic terahertz amplified modulators may have promising applications in terahertz technology, especially in communications [31].

References

- [1] M. Tonouchi, "Prospect of terahertz technology," in *Proc. IEEE 19th Int. Conf. Appl. Electromagn. Commun.*, 2007, pp. 1–4.
- [2] J. Federici and L. Moeller, "Review of terahertz and subterahertz wireless communications," *J. Appl. Phys.*, vol. 107, no. 11, 2010, Art. no. 111101.
- [3] J. Y. Suen, "Terabit-per-second satellite links: A path toward ubiquitous terahertz communication," *J. Infrared Millim. THz Waves*, vol. 7, no. 37, pp. 615–639, 2016.
- [4] P. Li *et al.*, "Design of tunable terahertz bandstop filter based on electrostatically actuated reconfigurable metamaterials," *Opt. Commun.*, vol. 392, pp. 263–267, 2017.
- [5] J. Sun *et al.*, "The effect of symmetry on resonant and nonresonant photoresponses in a field-effect terahertz detector," *Appl. Phys. Lett.*, vol. 106, no. 3, 2015, Art. no. 031119.
- [6] B. Sensale-Rodriguez, L. Liu, P. Fay, D. Jena, and H. G. Xing, "Power amplification at THz via plasma wave excitation in RTD-gated HEMTs," *IEEE Trans. THz Sci. Technol.*, vol. 3, no. 2, pp. 200–206, Mar. 2013.
- [7] H. O. Condori Quispe, J. J. Encomendero-Risco, H. G. Xing, and B. Sensale-Rodriguez, "Terahertz amplification in RTD-gated HEMTs with a grating-gate wave coupling topology," *Appl. Phys. Lett.*, vol. 109, no. 6, 2016, Art. no. 063111.
- [8] B. Sensale-Rodriguez, "Graphene-insulator-graphene active plasmonic terahertz devices," *Appl. Phys. Lett.*, vol. 103, no. 12, 2013, Art. no. 123109.
- [9] M. Salman, F. Gouider, H. Schmidt, Y. B. Vasilyev, R. Haug, and G. Nachtwei, "Terahertz photoresponse dependence on magnetic and electric fields in graphene-based devices," *Phys. Status Solidi C*, vol. 8, no. 4, pp. 1208–1210, 2011.
- [10] Y. Huang, S. Zhong, H. Yao, and D. Cui, "Tunable terahertz plasmonic sensor based on graphene/insulator stacks," *IEEE Photon. J.*, vol. 9, no. 1, Feb. 2017, Art. no. 5900210.
- [11] H.-T. Chen *et al.*, "Electronic control of extraordinary terahertz transmission through subwavelength metal hole arrays," *Opt. Express*, vol. 16, no. 11, pp. 7641–7648, 2008.
- [12] O. Paul *et al.*, "Polarization-independent active metamaterial for high-frequency terahertz modulation," *Opt. Express*, vol. 17, no. 2, pp. 819–827, 2009.
- [13] D. Shrekenhamer *et al.*, "High speed terahertz modulation from metamaterials with embedded high electron mobility transistors," *Opt. Express*, vol. 19, no. 10, pp. 9968–9975, 2011.
- [14] E. Hendry, M. J. Lockyear, J. G. Rivas, L. Kuipers, and M. Bonn, "Ultrafast optical switching of the THz transmission through metallic subwavelength hole arrays," *Phys. Rev. B*, vol. 75, no. 23, 2007, Art. no. 235305.
- [15] H.-T. Chen *et al.*, "Ultrafast optical switching of terahertz metamaterials fabricated on ErAs/GaAs nanoisland superlattices," *Opt. Lett.*, vol. 32, no. 12, pp. 1620–1622, 2007.
- [16] D. Roy Chowdhury *et al.*, "Dynamically reconfigurable terahertz metamaterial through photo-doped semiconductor," *Appl. Phys. Lett.*, vol. 99, no. 23, 2011, Art. no. 231101.
- [17] T. Vogel, G. Dodel, E. Holzhauer, H. Salzmann, and A. Theurer, "High-speed switching of far-infrared radiation by photoionization in a semiconductor," *Appl. Opt.*, vol. 31, no. 3, pp. 329–337, 1992.
- [18] B. Sensale-Rodriguez, P. Fay, L. Liu, D. Jena, and H. Xing, "Enhanced terahertz detection in resonant tunnel diode-gated hemts," *ECS Trans.*, vol. 49, no. 1, pp. 93–102, 2012.
- [19] C. Tripon-Canseliet *et al.*, "High dynamic range single channel sampling of wideband RF signals using ultra-fast nanoscale photoconductive switching," *Electron. Lett.*, vol. 52, no. 3, pp. 237–239, 2015.
- [20] C. Lu, Q. Fu, S. Huang, and J. Liu, "Polymer electrolyte-gated carbon nanotube field-effect transistor," *Nano Lett.*, vol. 4, no. 4, pp. 623–627, 2004.

- [21] P. W. Park, H. Y. Chu, S. G. Han, Y. W. Choi, G. Kim, and E.-H. Lee, "Optical switching mechanism based on charge accumulation effects in resonant tunneling diodes," *Appl. Phys. Lett.*, vol. 67, no. 9, pp. 1241–1243, 1995.
- [22] I. Coêlho, J. Martins-Filho, J. Figueiredo, and C. Ironside, "Modeling of light-sensitive resonant-tunneling-diode devices," *J. Appl. Phys.*, vol. 95, no. 12, pp. 8258–8263, 2004.
- [23] E. Brown, O. McMahon, L. Mahoney, and K. Molvar, "Spice model of the resonant-tunnelling diode," *Electron. Lett.*, vol. 32, no. 10, pp. 938–940, 1996.
- [24] B. L. Sharma and R. K. Purohit, *Semiconductor Heterojunctions*, vol. 5. Amsterdam, The Netherlands: Elsevier, 2015.
- [25] M. Dyakonov and M. Shur, "Shallow water analogy for a ballistic field effect transistor: New mechanism of plasma wave generation by dc current," *Phys. Rev. Lett.*, vol. 71, no. 15, pp. 2465–2468, 1993.
- [26] M. Dyakonov and M. Shur, "Detection, mixing, and frequency multiplication of terahertz radiation by two-dimensional electronic fluid," *IEEE Trans. Electron Devices*, vol. 43, no. 3, pp. 380–387, 1996.
- [27] I. Khmyrova and Y. Seijyou, "Analysis of plasma oscillations in high-electron mobility transistorlike structures: Distributed circuit approach," *Appl. Phys. Lett.*, vol. 91, no. 14, 2007, Art. no. 143515.
- [28] P. Burke, I. Spielman, J. Eisenstein, L. Pfeiffer, and K. West, "High frequency conductivity of the high-mobility two-dimensional electron gas," *Appl. Phys. Lett.*, vol. 76, no. 6, pp. 745–747, 2000.
- [29] D. M. Pozar, *Microwave Engineering*. Hoboken, NJ, USA: Wiley, 2009.
- [30] J. G. Proakis, M. Salehi, N. Zhou, and X. Li, *Communication Systems Engineering*. Englewood Cliffs, NJ, USA: Prentice-Hall, 1994, vol. 2.
- [31] M. Rahm, J.-S. Li, and W. J. Padilla, "THz wave modulators: A brief review on different modulation techniques," *J. Infrared Millim. THz Waves*, vol. 34, pp. 1–27, 2012.
- [32] T. Pearsall, "Ga 0.47 in 0.53 as: A ternary semiconductor for photodetector applications," *IEEE J. Quantum Electron.*, vol. 16, no. 7, pp. 709–720, Jul. 1980.
- [33] Q. Liu, A. Seabaugh, P. Chahal, and F. J. Morris, "Unified AC model for the resonant tunneling diode," *IEEE Trans. Electron Devices*, vol. 51, no. 5, pp. 653–657, May 2004.
- [34] T. Mozume and S. Gozu, "Photoreflectance study of InGaAs/AlAsSb coupled double quantum wells," *Physica Status Solidi C*, vol. 9, no. 2, pp. 334–337, 2012.